Selection of velocity profile and flow depth in granular flows

B. Andreotti and S. Douady
Laboratoire de Physique Statistique de l'Ecole Normale Supérieure, 24 rue Lhomond, 75231 Paris Cedex 05, France
(Received 20 October 2000; published 26 February 2001)

The dynamics of a two-dimensional pile constituted by spherical grains organized in parallel layers is investigated theoretically. Only three effects are taken into account in the model: driving by gravity, nonlocal dissipation due to shocks, and trapping of grains by the bumps of the underneath layer. This is sufficient to recover the basic properties of granular avalanches: the transition between static and flowing state is hysteretic; the pile does not flow on the whole height but only in a layer at the surface; the velocity profile inside the flowing layer is approximately linear and is followed by a creep motion in the (quasi) static part. The flow height increases as a function of the pile angle and tends to infinity for a critical angle φ_∞. The dependence of this critical angle with the static angle φ_s, the restitution coefficient ρ, and the moment of inertia J, is investigated.

DOI: 10.1103/PhysRevE.63.031305 PACS number(s): 83.80.Fg, 45.05.+x

I. INTRODUCTION

Although they are difficult to analyze, most of the basic properties of granular media are somehow easy to observe. For instance, most of us have already built a sand pile by pouring some sand on an horizontal surface. The sand accumulates at the top of the pile, which remains static until the angle φ of the free surface becomes locally larger than the static angle φ_s. Then, an avalanche spontaneously starts and rushes down the pile. It survives as long as the free surface angle remains larger than the dynamical angle φ_d. The dynamics of the avalanche appears to be very different from that of usual fluids since only a thin layer of grains is set into motion (Fig. 1). This behavior rises several problems still open up to now:

(i) What are the basic mechanisms leading to the subcritical transition between equilibrium and motion?

(ii) What selects the depth on which the sand flows?

(iii) What determines the velocity profile inside this layer?

Velocity profiles in avalanches were measured by Rajchenbach [1] in a rotating drum with a width of one grain diameter. He found that the velocity profiles were approximately linear [$\partial_z v \simeq \Gamma(\varphi)$] with a slight viscouslike curvature ($\partial_{zz} v < 0$) in the upper part and a slight creeping tail ($\partial_{zz} v > 0$). The same kind of profiles were obtained numerically by Azanza, Chevoir, and Maucharont [2] and Prochnow, Chevoir, and Albertelli [3] but with a larger curvature ($\partial_{zz} v < 0$). However, the existence of a static bottom was not observed in the numerical simulations: the grains were always rolling down to the rough bottom. For completeness, let us mention that velocity profiles were also measured in experiments on collisional flows down rough inclined planes [4,5], with the same conclusion.

We measured velocity profiles (Fig. 1) at the boundary of a quite large channel (100 grain diameters) by a (intercorrelation of images) method PIV. They exhibit a strong shear at the free surface followed in the lower part by a creep motion region as that observed by Komatsu *et al.* [6]. Again, the velocity profile is approximately linear but exhibits now a positive curvature ($\partial_{zz} v > 0$) so that the velocity gradient is maximum at the free surface. It is just the opposite of usual fluids in which the constraint and thus the velocity gradient are null at the free surface and maximum at the static boundary. This is very important since it proves that in granular flows the constraints are not only related to the strain tensor [1].

In a previous article [7] we have revisited the dynamics of a single grain rolling on a rough inclined surface. We have shown that this simple system already presents a subcritical bifurcation between equilibrium and motion similar to that of a whole sand pile. Three dynamical mechanisms were taken into account. The grain is driven downward by gravity but a part of its kinetic energy is dissipated each time it collides beneath a bump. The balance between these two effects determines a limit velocity. The two critical angles come from the trapping of the grain between the plane bumps. The static angle φ_s is the angle above which the trap disappears. The dynamical angle φ_d is the angle below which the limit velocity is not sufficient to escape from trapping.

The aim of this paper is to extend the previous model [7] to the case of several layers of grains, keeping the same three effects, gravity driving, dissipation by shocks, and potential trapping. We will examine the two problems previously risen: the selection of the flowing height and the shape of the velocity profile.

II. MODELING

Many effects can influence the dynamics of granular flows: the roughness, the elasticity, and the geometry of grains but also electrostatic interaction or humidity. However, three mechanisms are always present in any granular material: gravity, dissipation by the shocks between grains, and trapping of the grains between their neighbors. Our aim is to build a simple model in which *only these three effects play a role* and can be tuned independently.

We consider a two-dimensional pile constituted by spherical grains organized in parallel layers. All the quantities used in this paper are rescaled using the grains diameter d, their mass m, and the gravity field g ($d^{1/2}g^{-1/2}$ is the typical timescale). The lower layer $n=0$ is fixed and constitutes the rough plane on which the grains flow. The plane can be

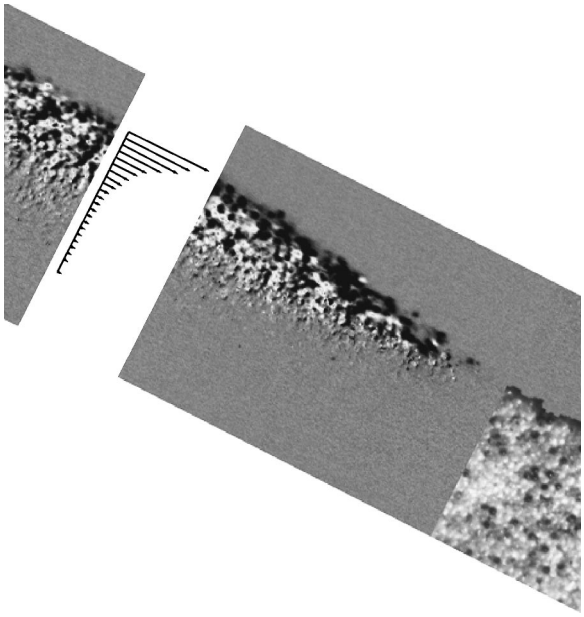

FIG. 1. During an avalanche, only a thin layer of grains flows. The velocity profile exhibits a large gradient in the bulk of the layer. At the interface between the static pile and the flowing layer, a region of creep motion can be observed. This instantaneous velocity profile was obtained by means of PIV in a channel of 100 grain diameters width.

inclined at an angle φ, which is the control parameter. Inside each layer n, the grains are separated by a fixed distance $2d \sin \varphi_s$ (Fig. 2).

A. Equations of motion

By assumption, the grains $n-1$ and n of successive layers are in permanent contact at point I_n. The position of the grain n relatively to the grain $n-1$ is specified by the angle θ_n (Fig. 2) between the perpendicular to the inclined plane and the vector joining the centers of mass ($\mathbf{G}_{n-1}\mathbf{G}_n = 2\mathbf{I}_n\mathbf{G}_n = \mathbf{u}_{\theta_n}$). The velocity of the grain n is thus

$$\mathbf{v}_n = \sum_{i=1}^{n} \dot{\theta}_i \mathbf{u}_{\theta_{i+\pi/2}}. \tag{1}$$

We assume that the grain n rolls without sliding around the beneath one $n-1$ so that its angular velocity is

$$\mathbf{\Omega}_n = 2\sum_{i=1}^{n} (-1)^{i+n} \dot{\theta}_i \mathbf{k}. \tag{2}$$

The motion is conservative except during the shocks. Introducing the moment of inertia J of a grain about its diameter, the kinetic energy T of the whole chain of grains reads:

$$T = \frac{1}{2} \sum_{i,j=1}^{N} \alpha_{i,j} [\cos(\theta_i - \theta_j) + (-1)^{i+j} J] \dot{\theta}_i \dot{\theta}_j \tag{3}$$

with $\alpha_{i,j} = [N+1-\max(i,j)]$. Its potential energy is

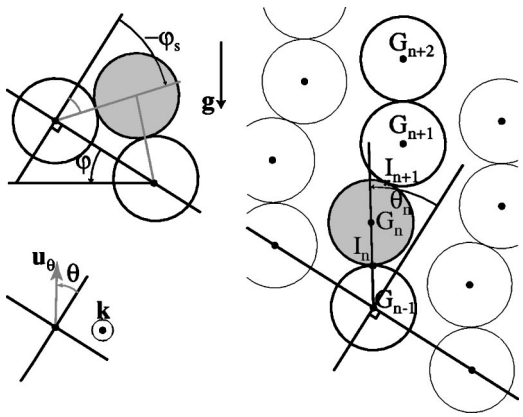

FIG. 2. The grain n is assumed to roll without sliding on the grain $n-1$ beneath it at the contact point I_n. The positions are specified by the angles θ_n, which vary from φ_s just after one shock down to $-\varphi_s$ just before the next one. The system is periodic along the direction of the layers so that only the dynamics of one chain of grains has to be computed.

$$U = -\sum_{i=1}^{N} (N+1-i)\cos(\theta_i - \varphi). \tag{4}$$

Finally, the equations of motion directly follows as a set of coupled equations labeled by n:

$$\sum_{i=1}^{N} \alpha_{i,n} [\cos(\theta_i - \theta_n) + (-1)^{i+n} J] \ddot{\theta}_i = \sum_{i=1}^{N} \alpha_{i,n} \sin(\theta_i - \theta_n) \dot{\theta}_i \dot{\theta}_n + (N+1-n)\sin(\theta_n - \varphi). \tag{5}$$

It is worth noting that the right-hand side is composed by two terms: an inertial term quadratic in $\dot{\theta}_i$ and the gravity term proportional to the number of beads above n.

When the grain l collides with the grain $l-1$, part of the kinetic energy is dissipated. We assume that the shock is instantaneous and that the forces are transmitted through the contact points I_n. To find the N independent quantities conserved during the shock, let us consider the subsystem $\{n, n+1, \ldots, N\}$. Except gravity, which can be neglected, the only external force on this subsystem is that exerted at the contact point I_n by the grain $n-1$. As a consequence, the angular momentum of the subsystem $\{n, n+1, \ldots, N\}$ about the point I_n is conserved. Denoting, respectively, by the subscripts $-$ and $+$ the quantities before and after the shocks, we obtain

$$\sum_{i=1}^{N} \alpha_{i,n} [\cos(\theta_i^- - \theta_n^+) + (-1)^{i+n} J] \dot{\theta}_i^- = \sum_{i=1}^{N} \alpha_{i,n} [\cos(\theta_i^+ - \theta_n^+) + (-1)^{i+n} J] \dot{\theta}_i^+ .$$

The relative position θ_l of the grain l changes during the shocks from $-\varphi_s$ to φ_s, if $\dot{\theta}_l$ is negative, and from φ_s to

$-\varphi_s$, if $\dot{\theta}_l$ is positive. The position θ_n of all the other grains remain the same before and after the shock. The previous expression can thus be simplified into

$$\sum_{i=1}^{N} \alpha_{i,n}[\cos(\theta_i^+ - \theta_n^+) + (-1)^{i+n} J](\dot{\theta}_i^+ - \dot{\theta}_i^-) = -2\alpha_{l,n} \sin(\theta_n^+)\sin(\varphi_s)|\dot{\theta}_l^-|. \quad (6)$$

The most important thing to note about these shocks is their nonlocality. The collisions are not binary but the whole chain of grains is involved: the flowing layer is not isolated and consequently its momentum is not conserved.

B. Simplified model

Investigating the effects of the dynamical mechanisms directly from Eqs. (5) and (6) governing the motion and the collisions is not an easy task. We will thus first simplify the model term by term.

The expression of the kinetic energy involves a projection factor $\cos(\theta_i - \theta_n)$, which remains almost constant during the motion. The first simplification is to approximate this factor by 1 so that the kinetic energy becomes: $T = \frac{1}{2}\Sigma_{i,j=1}^{N} \alpha_{i,j}[1 + (-1)^{i+j} J]\dot{\theta}_i \dot{\theta}_j$. As a consequence, the inertial term in the right-hand side of the equation of motion (5) disappears. This is justified by the fact that $\sin(\theta_i - \theta_n)$ is null on the average and leads to a simpler equation of motion:

$$\sum_{i=1}^{N} \alpha_{i,n}[1 + (-1)^{i+n} J]\ddot{\theta}_i = (N+1-n)\sin(\theta_n - \varphi).$$

Similarly, the restitution factor $\sin(\theta_n^+)$ in the right-hand side of the collision equation (6) could be thought of as being null on the average. This is true, except for the grain l, which collides with the one beneath. Indeed, the angle θ_l^+ is known to be equal to $-\varphi_s$ (or φ_s for a backward collision). After averaging over microscopic configurations, the second equation becomes

$$\sum_{i=1}^{N} \alpha_{i,n}[1 + (-1)^{i+n} J](\dot{\theta}_i^+ - \dot{\theta}_i^-) = -2(N+1-l)\sin^2(\varphi_s)\,\delta_{l,n}\dot{\theta}_l^-.$$

On the average, the grain l makes approximately $|\dot{\theta}_l|/2\varphi_s$ shocks per unit time. The discrete shocks can thus be replaced by a continuous friction force:

$$\sum_{i=1}^{N} \alpha_{i,n}[1 + (-1)^{i+n} J][\ddot{\theta}_i]_{\text{shocks}} \simeq -(N+1-n)\frac{\sin^2(\varphi_s)}{\varphi_s}|\dot{\theta}_n|\dot{\theta}_n.$$

We finally obtain an equation set governing the motion:

$$M_{n,i}\ddot{\theta}_i = \sin(\theta_n - \varphi) - \rho|\dot{\theta}_n|\dot{\theta}_n, \quad (7)$$

where the restitution coefficient ρ is approximately equal to $\sin^2(\varphi_s)/\varphi_s$ and where the matrix M is given by $M_{n,i} = [1 + (-1)^{i+n} J][N+1-\max(i,n)]/(N+1-n)$.

C. Discussion

The model fully generalizes the case of one grain on a rough bottom investigated in a previous article [7]. For $N=1$ the equation of motion reduces to $(1+J)\ddot{\theta} = \sin(\theta - \varphi) - \rho|\dot{\theta}|\dot{\theta}$, which already leads to a subcritical transition between equilibrium and motion. This characteristic is due to the fact that the grain can remain static in the dip between underlying grains and, when flowing, that it has to keep enough kinetic energy after each collision to pass above these grains [7]. In Eq. (7), this trapping effect is related to the fact that the gravity term $\sin(\theta - \varphi)$ has a drawback effect in a part of the trajectory (for $\varphi_s > \theta > \varphi$).

The case of several stacked layers is more complicated because the shock of one grain has an effect on all the other layers (nonlocal shocks). This can be seen in Eq. (7) where the left-hand side involves the angular acceleration of all the chain of grains. This introduces an essential difference with Bagnold's model [8] in which the shocks are assumed to be binary and have an effect only for the two layers colliding. This nonlocality makes the resolution hardly possible theoretically.

Keeping the dissipation localized at the shocks, we would have to perform a molecular dynamics type of simulation. To avoid this, the dissipation has been replaced by a friction quadratic in $\dot{\theta}$ acting continuously along the grain trajectory. This simplification allows a fixed time step simulation. It was checked in the case of a single grain that the overall dynamics does not change. On the other hand, to keep the trapping effect, the force term was of course not similarly averaged.

The second interest of the simplification [Eq. (7)] is to allow the tuning of each effect separately. The dissipation is controlled by the coefficient ρ. The trapping of the grains is related to the oscillation of the gravity term $\sin(\theta_n - \varphi)$. It is thus controlled by φ_s, i.e., by the compacity of the pile. The accumulation restitution of rotation energy is controlled by the moment of inertia J. Finally, the effect of the rough fixed bottom depends on the total number of layers N.

III. RESULTS

A. Velocity profiles

We integrate the model numerically using a fourth-order Runge Kutta method. As a reference case, we chose $\rho = 1$, $\varphi_s = 40°$, $J = 0.5$, and $N = 50$. A visualization of the pile is shown on Fig. 3 for $\varphi = 24°$ together with the mean velocity profile. The first thing to note is that the grains only flow in the upper part of the pile: as in a actual sand pile (Fig. 1), there exists a quasistatic part. The second is the similarity between the actual velocity profile and that given by the model. It is characterized by a strongly sheared layer near the free surface together with a slight creep motion in the bottom

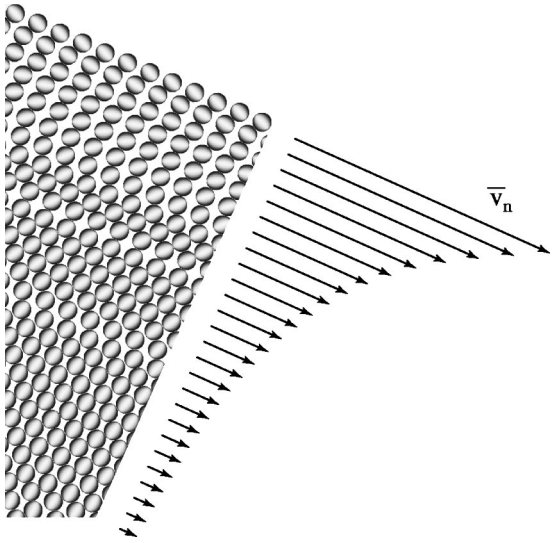

FIG. 3. Left: a visualization of the flowing layer ($\varphi=24°$). Right: the corresponding mean velocity profile.

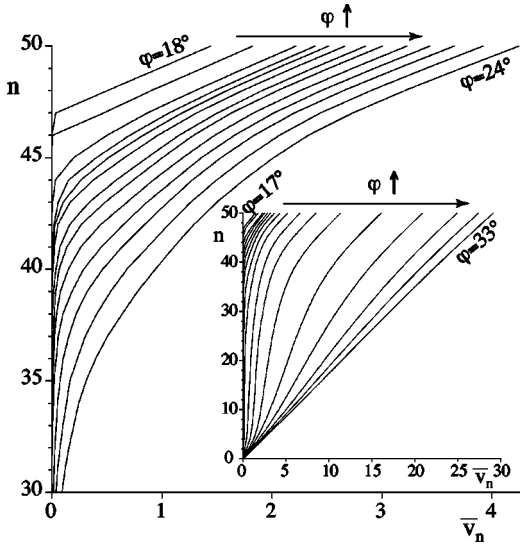

FIG. 4. Evolution of the mean velocity profile with the angle φ by steps of 0.5°. The flowing height increases with the angle φ. The creep motion reaches the bottom plane around $\varphi=25°$. Above this value (inset), the velocity profile changes and becomes again nearly linear above $\varphi=33°$. The velocities are rescaled by $g^{1/2}d^{1/2}$.

part. The curvature is the same as in the experiment ($\partial_{zz}v>0$) corresponding to the fact that the velocity gradient is maximum at the free surface.

Looking at Fig. 3, one can observe that the first seven layers ($n=N-6$ to $n=N$) are moving. This region corresponds on the mean velocity profile to the large shear region at the free surface. Below, only two layers are moving ($n=N-9$ and $n=N-15$) all the others being trapped. At the same depth, the mean profile does not exhibit any discontinuity. The creep motion in this region is thus very intermittent. One layer starts jumping above the one beneath but then remains trapped for some time. A different layer makes a relative motion of one grain and so on. Due to this irregular motion, we will focus on quantities averaged over 1000 unit times.

The evolution of the mean velocity profile with the plane angle φ is shown in Fig. 4. It turns out that the flowing height increases with the angle, between $\varphi=18°$ and $\varphi=25°$. In this angle range, the velocity profile remains approximately linear in the bulk but the creep motion region is more and more extended. Around $\varphi=25°$, the flow reaches the bottom (Fig. 4, inset). Above, the velocity profile changes drastically and becomes again linear at much larger angles ($\varphi>32°$), with just the velocity gradient increasing with the plane angle φ.

B. Flow height

It is interesting to characterize the flow by a few parameters such as the flow height H and the mean velocity gradient Γ inside the flowing layer. However, without a precise model of the creeping tail, this is difficult to do. A first possibility is to use simply the velocity gradient at the free surface $\Gamma_s=v_N-v_{N-1}$ (Fig. 5). The typical flow height H_s can then be defined using the velocity at the free surface $v_N=\Gamma_s H_s$. This corresponds to approximate the velocity profile by its tangent at the free surface (dashed line on Fig. 5).

Another way of defining the flow depth is to use integral quantities like the flow rate $Q=\Sigma_{n=1}^{N}v_n$ and the translation kinetic energy $E=\Sigma_{n=1}^{N}v_n^2$. Dimensionally, we obtain a length $H\propto Q^2/E$ and a frequency $\Gamma\propto E^2/Q^3$. The prefactors can be adjusted to recover the right flowing depth and velocity gradient when the velocity profile is linear (solid line in Fig. 5):

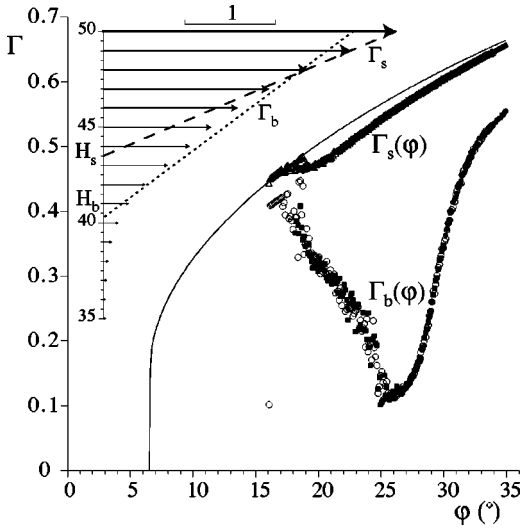

FIG. 5. Velocity gradient Γ as a function of the angle φ. Γ_s is the velocity gradient at the free surface (dashed line on the inset). Γ_b is the bulk mean gradient defined using the momentum Q and the kinetic energy E (dotted line on the inset). The black points are obtained by increasing slowly the angle $\varphi'(t)=+10^{-5}$, the white ones by decreasing the angle $\varphi'(t)=-10^{-5}$. The solid line corresponds to the velocity gradient of a single grain on a rough bottom ($N=1$). The velocity gradients are rescaled by $g^{1/2}d^{-1/2}$.

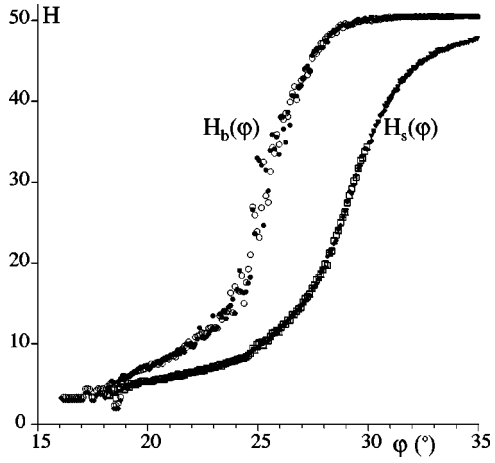

FIG. 6. Flow depth H as a function of the angle φ. H_b and H_s are, respectively, estimated from the velocity profile in the bulk and at the free surface (see Fig. 5). As in Fig. 5, the black points are obtained by increasing slowly the angle $\varphi'(t)=+10^{-5}$, the white ones by decreasing the angle $\varphi'(t)=-10^{-5}$. The heights are rescaled by the grains diameter d.

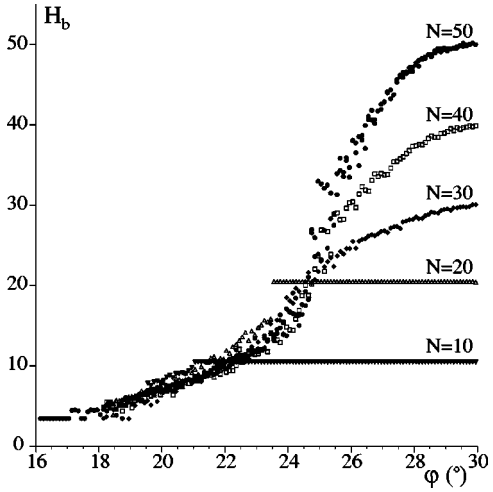

FIG. 7. Flow depth H as a function of the angle φ for different total height N (10, 20, 30, 40, and 50). As previously, the heights are given in number of grains.

$$H_b=\frac{4Q^2}{3E}, \quad \Gamma_b=\frac{9E^2}{8Q^3}. \tag{8}$$

The evolution of the velocity gradient Γ and of the flowing depth H with the angle φ are plotted in Figs. 5 and 6. The flow height defined from the velocity profile at the free surface (H_s) and in the bulk (H_b) have globally the same evolution. They increase gradually with the angle φ from $H=3$ at $\varphi=16°$ to the total number of layers $H=N=50$ at large angle. The mean velocity gradient in the bulk (Γ_b) and at the free surface (Γ_s) evolve very differently. At $\varphi=16°$, the velocity profile is strictly linear: Γ_b and Γ_s are thus equal. Above, Γ_b decreases due to the development of the creep motion tail. A sudden change of behavior appears at $\varphi=25°$, angle at which the creep motion reaches the fixed bottom. Above, Γ_b increases rapidly and becomes asymptotically equal to Γ_s at very large angles, corresponding to the fact that the velocity profile tends towards linearity. On the other hand, the velocity gradient at the free surface remains almost equal to the velocity of one grain ($N=1$) on a fixed bottom (solid line on Fig. 5) meaning that it does not feel much from the motion in the bulk. It can be seen in Fig. 6 that the crisis around $\varphi=25°$ results in a fast increase of the flow height H with the angle.

As a first approximation, the total number of layers N modifies only the height at which H saturates at large angles (Fig. 7). It can also be noted that the saturation is sharper for thin layers ($N=10$ and $N=20$). It is remarkable that the sudden increase of the flow height approximately occurs at the same angle φ_c. This suggests the existence of a divergence of $H(\varphi)$, in the limit of a very large number of layers.

It is clear that the selection of the flow depth can be ascribed to trapping i.e., to the fact that grains should have a sufficient kinetic energy to climb the bumps of the underneath layer. More precisely, a grain of the layer $N+1-H$ has to lift up the $(H-1)$ grains located above it. It has thus to escape from a potential trap whose depth $E=gH[1-\cos(\varphi_s-\varphi)]$ increases linearly with H. If we assume that the other layers do not help the grain to escape from trapping, i.e., that they do not transmit kinetic energy to it, the last grain to flow has just enough kinetic energy ($\simeq\Gamma^2$) to escape from the potential trapping. The flowing height is then given by $H\simeq\Gamma^2/[1-\cos(\varphi_s-\varphi)]$, which predicts an increase of H with φ and a divergence at $\varphi=\varphi_s$. The divergence of H is indeed observed, but for a smaller angle φ_c. In fact, all the layers are coupled so that the upper layers help the lower layers to escape from trapping. But this help is not enough to balance the increase of the potential trap; the depth obtained from the numerical integration of the model is larger than that estimated under the hypothesis of uncoupled layers.

C. Reversibility, Hysteresis

The white points in Figs. 5 and 6 are obtained by decreasing the angle φ continuously at the slow rate of $\varphi'(t)=-10^{-5}\,\mathrm{rad\,g^{1/2}\,d^{-1/2}}$. The initial condition was prepared randomly at $\varphi=35°$ and the equations of motion were integrated over 1000 unit times before decreasing the angle. To check that the pile was always at statistical equilibrium, we investigated the reversibility of the curve by preparing the initial condition randomly at $\varphi=16°$ and by increasing the angle φ at the rate $\varphi'(t)=10^{-5}\,\mathrm{rad\,g^{1/2}\,d^{-1/2}}$. The result, in black points in Figs. 5 and 6, shows very clearly that above $\varphi=16°$ the system is reversible.

This is evidently not the case if we start from a pile initially at rest. In that case, the motion starts spontaneously at the static angle φ_s, above which the trapping disappears. Between $\varphi=16°$ and $\varphi=\varphi_s=40°$, the equilibrium is metastable and one rolling grain is sufficient to initiate the motion of the whole layer. Finally, below $\varphi=\varphi_d\simeq16°$, the flow stops [9]. We thus recover, in the present model, the hysteresis between equilibrium and flowing observed in actual sand piles.

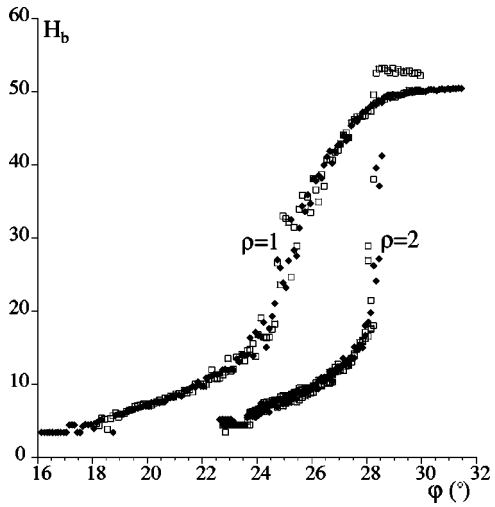

FIG. 8. Flow depth H as a function of the angle φ for two different restitution coefficients ($\rho=1$ and $\rho=2$). As previously, the heights are rescaled by the grains diameter d.

D. Parametric study of the flowing height

We investigate in this section the effect of the static angle φ_s, of the restitution coefficient ρ and of the moment of inertia J on the dynamics of the pile. For all the sets of parameters investigated, we recovered qualitatively the behavior previously described. We will thus limit ourselves to study, parametrically, the flowing height $H_b(\varphi)$.

The relation between the flowing height and the angle is shown in Fig. 8 for two different restitution coefficients ρ. The global evolution is the same but the divergence and the saturation are much sharper for $\rho=2$ than for $\rho=1$. For a larger dissipation rate, both the angle φ_d above which the motion is possible and that φ_c at which H diverges, are larger. On the other hand, the range of angles for which the pile flows on a finite depth is smaller (9° for $\rho=1$ against 5.5° for $\rho=2$). The increase of the critical angles with the dissipation rate ρ is indirectly related to the trapping. When ρ is increased, the kinetic energy globally decreases. As a consequence, a larger angle is necessary to recover a kinetic energy sufficient to escape from the trapping.

Similarly, we observe in Fig. 9 that the two critical angles increase with the static angle φ_s. This time, the range of angles for which a static part exists also increases with φ_s. Changing the static angle φ_s allows to change the depth of the traps without changing the kinetic energy. Again, for a larger static angle φ_s, a larger kinetic energy is necessary to escape from the trapping and thus a larger angle.

The moment of inertia J of the grains about their diameter controls the accumulation and the restitution of rotation kinetic energy. When J is increased, the angle φ_c at which H seams to diverge decreases (Fig. 10). As for the dependence of ρ and φ_s, this is due to the trapping. An increase of J induces a regulation of the kinetic energy by the rotation: the grains become less sensitive to the oscillation of the gravity force. Thus, for a large moment of inertia J, a lower angle is necessary to escape from the traps.

This parametric study shows that the selection of the flow depth is governed by the trapping effect: if trapping is increased (by φ_s) or kinetic energy reduced (by ρ or J), both the angle φ_d above which the motion is possible and the angle φ_c for which the flow height diverges, increase.

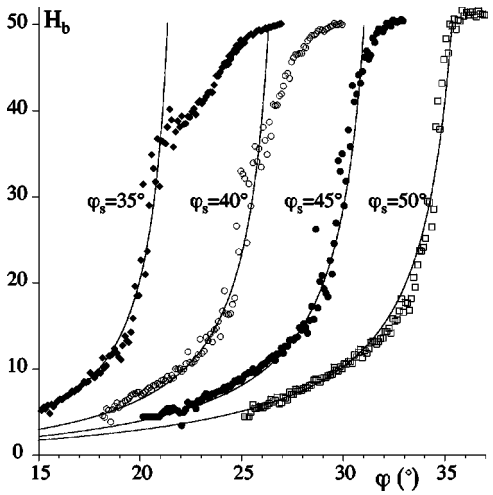

FIG. 9. Flow depth H as a function of the angle φ for different static angle φ_s (35°, 40°, 45°, and 50°) and thus different compacities. As a guideline, a fit by the function $\alpha \sin(\varphi)/\sin(\varphi-\varphi_c)$ is superimposed to the numerical points. The divergence angle φ_c increases with φ_s but α remains constant ($\alpha \simeq 2.5$). As previously, the heights are rescaled by the grains diameter d.

IV. CONCLUSION

We have proposed in this paper a crude model of sand piles constituted by parallel layers of grains. Only three mechanisms are taken into account: gravity, dissipation by nonlocal shocks, and trapping of the grains. The models allows nonetheless to recover the subcritical transition between static equilibrium and motion observed in actual sand piles

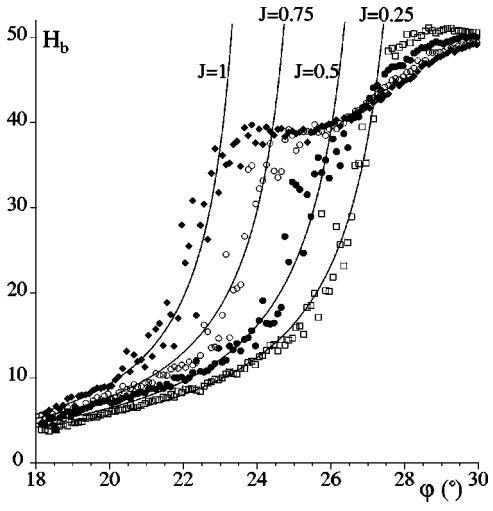

FIG. 10. Flow depth H as a function of the angle φ for different moments of inertia J (0.25, 0.5, 0.75, and 1). As in Fig. 9, a fit by the function $\alpha \sin(\varphi)/\sin(\varphi-\varphi_c)$ is superimposed to the numerical points. The divergence angle φ_c increases when J is decreased but α is constant as previously ($\alpha \simeq 2.5$). As previously, the heights are rescaled by the grain diameter d.

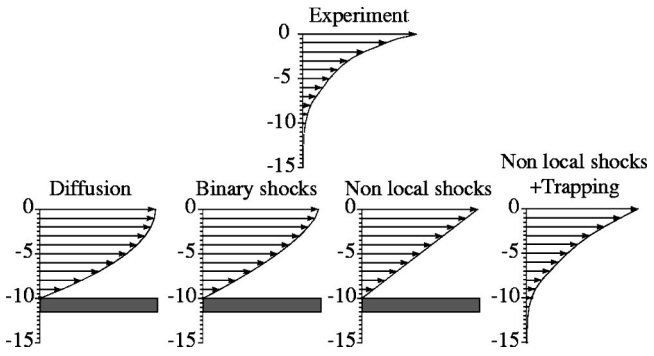

FIG. 11. In an actual sand pile, the flow is limited to a strongly sheared layer at the free surface (top). Depending on the nature of the dissipation, the velocity profile is different; for a viscous diffusion (thermal binary shocks, left), for binary collisions as in Bagnold's model (center left), and for nonlocal shocks (center right). These three models do not predict any internal limit to the flow depth. To recover this behavior, both nonlocal shocks and trapping of grains between its underneath neighbors have to be taken into account (present model, right).

but also the selection of a finite flow depth and the shape of the velocity profile.

The velocity profile inside a dense granular flow is different from that of a viscous fluid $[v \propto 1-(z/H)^2]$ by two properties: there exists a quasistatic part and the velocity gradient is maximum at the free surface. A viscous fluid flows down to the fixed bottom and the velocity gradient is null at the surface (Fig. 11). In the later case the velocity profile is derived from the viscous interaction between the fluid layers. This viscous coupling can be described as the exchange of momentum due to binary shocks of molecules induced by thermal agitation. Bagnold [8] proposed an adapted description, the collisional granular flow model, in which the shocks are not induced by thermal agitation but by the velocity difference of the grains themselves. This gives a viscosity (the momentum diffusion coefficient) no longer constant but proportional to the velocity gradient. The resulting velocity profile $[v \propto 1-(z/H)^{3/2}]$ is still very different from that measured in dense flowing layers (Figs. 1 and 11). Other adaptations could be thought as to change the relation between the stress and the strain to obtain the good profile. However, in any continuous model with a local stress strain relation, the shear stress (the constraints) should be null at the free surface and the shear strain should thus vanish at the free surface. Following the conclusions of Rajchenbach, Clement, and Duran [1], any model based on a local stress strain relation is inconsistent with experimental observations (Figs. 1 and 11).

In the present model, the shape of the velocity profile is recovered. To discriminate between the effect of the nonlocal shocks and that of the trapping, we can look at the result obtained when we average the equation of motion (7) to suppress the trapping. During motion, the gravity term $\sin(\theta_n-\varphi)$ oscillates and *changes sign*; it is the existence of this drawback force at some places that allows static positions. The average of this term over microscopic configurations is proportional to $-\sin(\varphi)$. If we replace it in the equations of motion (7), steady flows are immediately obtained; the velocity profile is linear with a velocity gradient Γ proportional to $\dot{\theta}_n \propto [\sin(\varphi)/\rho]^{1/2}$ and without a static part (Fig. 11).

From this simple comparison, we can conclude that

(i) the existence of a strong gradient at the free surface is not due to trapping but to the nonlocality of the shocks: when one grain collides a second grain, it looses a part of its momentum but this momentum is not transmitted to the second grain. It is transmitted through the whole chain of forces to the rigid bottom. The importance of the dissipation nonlocality is confirmed by the observation that the velocity gradient at the free surface is almost insensitive to the dynamics of the grains beneath it. Indeed, it is approximately equal to the velocity of one grain on a rough plane, as if each layer of grains was rolling on a fixed one [1].

(ii) in the absence of a drawback force at some places, the grains cannot remain at rest. The selection of a flowing depth is thus directly related to the trapping of the grains in the holes of the underneath layer. More precisely, it is due to the fact that the trapping potential increases linearly with the depth while the kinetic energy relatively to the underneath layer is almost that of one grain.

(iii) the velocity profile is strictly linear in the absence of trapping while it exhibits a creeping tail in the full model (Fig. 11). The creeping tail is thus also a signature of trapping.

As a conclusion, this model reproduces the velocity profile observed experimentally (including the maximum shear at the surface and the creeping tail), and the selection of a finite flow depth. Its simplicity allows to show that the strong shear can be ascribed to the equilibrium between gravity driving and dissipation by nonlocal shocks, and that the creeping tail and the finite depth can be ascribed to the trapping effect. It could be tempting to tune this model and introduce further effects to reproduce more closely some experimental results. However, it presents internal limitations due to its fixed geometry. Moreover, most of the velocity profiles measured experimentally could suffer from the rigid glass boundary introduced for side visualization. The detailed theoretical description of this velocity profile is also difficult [10,11].

It is more interesting to see the present model as a tool to understand the origin of several particularities of granular flows, and to use its general results to improve continuous models. For instance, the BCRE models [12,13], which consider equations governing the flow layer evolution, explicitly assume that the velocity profile is constant and do not take into account the hysteresis between static and flowing states (the trapping). But another type of model (known as DAD's) [14,15] uses the assumption of a linear velocity profile, closer to the results presented here. The predictions of these different models should thus be closely compared with experimental observations to investigate the influence of the different mechanisms (velocity profile, trapping...) on inhomogeneous flows like avalanches.

ACKNOWLEDGMENTS

The authors wish to thank A. Daerr, L. Quartier, and Y. Couder for many stimulating discussions about this work.

[1] J. Rajchenbach, E. Clément, and J. Duran, in *Fractal Aspects of Materials*, edited by F. Family, MRS Symposium Proceedings No. 367 (Materials Research Society, Pittsburgh, 1995), p. 525; J. Rajchenbach, in *Physics of Dry Granular Media*, edited by H. Hermann (Kluwer Academic, Dordrecht, 1998), p. 421.

[2] E. Azanza, F. Chevoir, and P. Moucheront, in *Powders and Grains*, edited by R. Behringer and J. Jenkins (A. A. Balkema, Rotherdam, 1997).

[3] M. Prochnow, F. Chevoir, and M. Albertelli, in *13th International Conference on Rheology* (unpublished).

[4] E. Azanza, F. Chevoir, and P. Moucheront, J. Fluid Mech. **400**, 199 (1999).

[5] C. Ancey, P. Evesque, and P. Coussot, J. Phys. I **6**, 725 (1996).

[6] T. S. Komatsu, S. Inagaki, N. Nakagawa, and S. Nasuno, e-print cond-mat/0008086.

[7] L. Quartier, B. Andreotti, A. Daerr, and S. Douady, Phys. Rev. E **62**, 8299 (2000).

[8] R. A. Bagnold, Proc. R. Soc. London, Ser. A **225**, 49 (1954).

[9] The situation is in fact more complicated. Indeed, for $\varphi < 6.5°$, any initial condition relaxes towards equilibrium but between $\varphi = 6.5°$ and $\varphi = 16°$ the pile remains in one of four metastable states: the motion of the two last layers, the motion of only the last but one layer, the motion of only the last layer, or all the layers at rest. These four configurations survive at long time if they are not disturbed. Starting from a flowing layer prepared at 16° and decreasing the angle φ the pile freezes in any of these four configurations depending on the history. This behavior is not generic and is only due to the quasicrystalline structure of the model: when the number of degrees of freedom is lower than three, the system stabilizes on a simple periodic motion. We considered in the article that the dynamical angle φ_d was the angle above which the flow is reversible.

[10] P. Mills, D. Loggia, and M. Tixier, Europhys. Lett. **45**, 733 (1999).

[11] J. Jenkins and F. Chevoir (unpublished).

[12] J. P. Bouchaud, M. Cates, J. R. Prakash, and S. F. Edwards, J. Phys. I **4**, 1383 (1994).

[13] T. Boutreux, E. Raphael, and P. G. de Gennes, Phys. Rev. E **58**, 4692 (1998).

[14] S. Douady, B. Andreotti, and A. Daerr, Eur. Phys. J. B **11**, 131 (1999).

[15] A. Aradian, E. Raphal, and P.-G. de Gennes, Phys. Rev. E **60**, 2009 (1999).